Applied and Environmental Microbiology, Nov. 2011, p. 7984–7997 Vol. 77, No. 22
0099-2240/11/$12.00 doi:10.1128/AEM.05374-11

Metabolome Remodeling during the Acidogenic-Solventogenic Transition in *Clostridium acetobutylicum*▽†

Daniel Amador-Noguez,[1] Ian A. Brasg,[1,2] Xiao-Jiang Feng,[2] Nathaniel Roquet,[1,2] and Joshua D. Rabinowitz[1,2]*

Lewis Sigler Institute for Integrative Genomics, Princeton University, Princeton, New Jersey 08544,[1] and Department of Chemistry, Princeton University, Princeton, New Jersey 08544[2]

Received 5 May 2011/Accepted 8 September 2011

The fermentation carried out by the biofuel producer *Clostridium acetobutylicum* is characterized by two distinct phases. Acidogenesis occurs during exponential growth and involves the rapid production of acids (acetate and butyrate). Solventogenesis initiates as cell growth slows down and involves the production of solvents (butanol, acetone, and ethanol). Using metabolomics, isotope tracers, and quantitative flux modeling, we have mapped the metabolic changes associated with the acidogenic-solventogenic transition. We observed a remarkably ordered series of metabolite concentration changes, involving almost all of the 114 measured metabolites, as the fermentation progresses from acidogenesis to solventogenesis. The intracellular levels of highly abundant amino acids and upper glycolytic intermediates decrease sharply during this transition. NAD(P)H and nucleotide triphosphates levels also decrease during solventogenesis, while low-energy nucleotides accumulate. These changes in metabolite concentrations are accompanied by large changes in intracellular metabolic fluxes. During solventogenesis, carbon flux into amino acids, as well as flux from pyruvate (the last metabolite in glycolysis) into oxaloacetate, decreases by more than 10-fold. This redirects carbon into acetyl coenzyme A, which cascades into solventogenesis. In addition, the electron-consuming reductive tricarboxylic acid (TCA) cycle is shutdown, while the electron-producing oxidative (clockwise) right side of the TCA cycle remains active. Thus, the solventogenic transition involves global remodeling of metabolism to redirect resources (carbon and reducing power) from biomass production into solvent production.

The anaerobic bacterium *Clostridium acetobutylicum* is a promising biofuel producer due to its capacity to ferment a variety of carbohydrates into acetone, butanol, and ethanol. The metabolism of this organism is characterized by two sequential phases. The first, the acidogenic phase, occurs during exponential growth and involves the rapid production of acids (acetate and butyrate). The second, the solventogenic phase, occurs as cell growth slows down and involves the production of solvents (butanol, acetone, and ethanol) and the partial re-assimilation of previously produced acids (12, 34). A comprehensive understanding of the mechanisms that control the transition into the solventogenic state would be an important step toward the commercial production of solvents using this anaerobic bacterium. Despite numerous research efforts, however, they remain incompletely understood (1, 13, 19, 33).

Initial studies of the acidogenic-solventogenic transition focused on investigating the biochemistry and transcriptional regulation of the pathways directly involved in acid and solvent production (12, 18, 21, 25). The acidogenic/solventogenic pathways, however, constitute only a fraction of the metabolic network, and their functionality relies on the supply of substrates (e.g., acetyl coenzyme A [acetyl-CoA], ATP, NADH, and NADPH) from core metabolic pathways. Therefore, it is reasonable to think that widespread metabolic changes are integral to the solventogenic transition. After the publication of the genome sequence of *C. acetobutylicum*, several transcriptomic studies have been performed with the purpose of gaining a more global understanding of the solventogenic transition (1, 24, 26). These studies have shown that, in addition to the expected changes in acid and solvent producing genes, significant transcriptional alterations in a large number of primary metabolic genes (such as glycolysis or amino acid biosynthesis pathways) also take place during the solventogenic transition. However, due to the complex nature of these alterations and the regulation of metabolism also at many other levels, the transcriptional data alone was insufficient to determine overall metabolic changes.

In the present study, we used metabolomics, isotope tracers, and quantitative flux modeling to directly map the metabolic events associated with the acidogenic-solventogenic transition. We observed a remarkably ordered series of metabolite concentration changes, involving almost all measured metabolites, as the fermentation progresses from acidogenesis to solventogenesis. Notably, these alterations were not restricted to the acidogenic/solventogenic pathways but encompassed core metabolic pathways such as glycolysis, the tricarboxylic acid (TCA) cycle, and amino acid biosynthesis. We also discovered that fluxes through some of these pathways, such as the reductive branch of the TCA cycle and amino acid biosynthesis, are greatly reduced during the transition. The overall effect of these changes is to redirect resources from biomass production into solvent production. Implications for possible metabolic

* Corresponding author. Mailing address: Department of Chemistry and Lewis Sigler Institute for Integrative Genomics, Princeton University, Princeton, NJ 08544. Phone: (609) 258-8985. Fax: (609) 258-3565. E-mail: joshr@princeton.edu.

† Supplemental material for this article may be found at http://aem.asm.org/.

▽ Published ahead of print on 23 September 2011.

regulation points that could be exploited to enhance solvent production are discussed.

MATERIALS AND METHODS

Media, culture conditions, and metabolite extraction. Inoculum preparation, batch fermentations, and metabolite extractions were performed inside an environmental chamber (Bactron IV SHEL LAB anaerobic chamber) with an atmosphere of 90% nitrogen, 5% hydrogen, and 5% carbon dioxide. The minimal medium formulation used in batch fermentations was as follows: KH_2PO_4, 2 g/liter; K_2HPO_4, 2 g/liter; $MgSO_4 \cdot 7H_2O$, 0.2 g/liter; NH_4Cl, 1.5 g/liter; biotin, 0.13 mg/liter; $FeSO_4 \cdot 7H_2O$, 32 mg/liter; 4-aminobenzoic acid, 0.16 mg/liter; and glucose, 60 g/liter (34).

For the preparation of batch fermentations, *C. acetobutylicum* ATCC 824 single colonies were picked from agar-solidified reinforced clostridial medium (RCM; Difco), resuspended in liquid RCM, heat-treated at 80°C for 20 min and grown to saturation overnight. This overnight culture was then used to inoculate (1:100 dilution) a liquid minimal media culture to an initial optical density at 600 nm (OD_{600}) of 0.03. When this liquid culture reached mid-exponential phase (OD_{600} of ~ 0.8), it was used to inoculate (1:25 dilution) a bioreactor (working volume, 400 ml) to an initial OD_{600} of 0.03. The fermentation was held at pH 4.7 by the addition of 1 N KOH. Intracellular metabolite samples were collected by rapidly (3 to 5 s) filtering 0.5 to 5 ml (dependent on cell density) of culture through 47-mm-diameter round hydrophilic nylon filters (Millipore catalog no. HNWP04700). Filters containing the cells are then immediately submerged into 1.5 ml of −20°C acetonitrile-methanol-water (40:40:20), which quenches metabolism and extracts metabolites (27, 36). The filtering and quenching steps were performed inside the anaerobic chamber described above. The filters were then washed with extraction solvent, the cellular extractions were transferred and centrifuged in Eppendorf tubes, and the supernatant was collected and stored at −20°C until analysis. An additional method, direct quenching (8), was used for the preparation of the metabolite samples for "fermentation B" shown in Fig. S2 in the supplemental material. The direct quenching method involves sampling 1 volume of culture and mixing it with 4 volumes of −20°C extraction solvent (acetonitrile-methanol [1:1]). The cellular extractions were then centrifuged, and the supernatant was collected and stored at −20°C until analysis. Medium samples for extracellular metabolite measurements were collected by filtering 3 ml of culture and stored at −20°C until analysis. Cellular growth was monitored based on the OD_{600} and by determining cell dry weight.

Metabolite measurements. Cell extracts and filtered medium samples were analyzed by reversed-phase, ion-pairing liquid chromatography coupled by electrospray ionization (ESI; negative mode) to a high-resolution, high-mass-accuracy mass spectrometer (Exactive; ThermoFisher) operated in full scan mode for the detection of targeted compounds based on their accurate masses (31). This analysis was complemented with liquid chromatography coupled by ESI (positive and negative mode) to Thermo TSQ Quantum triple quadrupole mass spectrometers operating in selected reaction monitoring mode (5, 30). Hydrophilic interaction chromatography was used for positive-mode ESI, and ion-pairing reversed-phase chromatography was used for negative-mode ESI. Amino acids were derivatized with benzyl chloroformate before their quantitation by negative-mode liquid chromatography (LC)-ESI-tandem mass spectrometry (MS/MS) (28). For the quantitation of major fermentation products (i.e., butyrate, acetate, butanol, acetone, and ethanol), we used cryoprobe-assisted ^{1}H-nuclear magnetic resonance (^{1}H-NMR) spectroscopy (10, 23).

The determination of absolute intracellular metabolite concentrations was performed using an isotope ratio-based approach described previously (7). Briefly, universally labeled [^{13}C]glucose minimal medium is used in inoculum preparation and fermentation batch cultures. Under these conditions nearly complete isotopic enrichment is attained. Metabolite samples are then collected using quenching solvent containing known concentrations of unlabeled internal standards. The concentrations of metabolites in the cells can be then calculated using the ratio of labeled endogenous metabolite to nonlabeled internal standard. The intracellular aqueous volume of *C. acetobutylicum* cells has been previously reported (40).

For all hierarchical clustering analyses, the data were clustered by metabolites using Pearson correlation (14) and visualized using TreeView (38).

Quantitative flux analysis. To investigate the remodeling of central metabolic fluxes during solventogenesis, we followed the dynamics of incorporation of labeled glucose into intracellular metabolites. Universally ^{13}C-labeled glucose was added into mid-exponential-phase or mid-solventogenic-phase cultures in a matching amount to the nonlabeled glucose remaining in the media to reach a 1:1 ratio between ^{13}C-labeled and nonlabeled glucose. At defined time points (e.g., 1, 2, 3, 5, 7, 10, 15, 30, and 60 min) after the addition of [^{13}C]glucose, the metabolism was quenched, and cell extracts were prepared and analyzed. The multiple isotope-labeled forms produced by the ^{13}C labeling were monitored simultaneously by LC-MS (30, 31). In all experiments, the labeling data were corrected for natural abundance of ^{13}C in nonlabeled substrates and for the ^{12}C impurity present in ^{13}C-labeled substrates in a similar fashion as reported previously (7, 42).

We used kinetic flux profiling (KFP) to obtain a quantitative estimate of metabolic fluxes from the kinetics of incorporation of ^{13}C-labeled glucose into downstream metabolites during acidogenesis and solventogenesis. The KPF methodology has been previously described in detail (43). Briefly, the main concept is that when an external isotopically labeled nutrient such as ^{13}C-labeled glucose is added to the media, for a given metabolite X downstream of glucose assimilation, unlabeled X (X^U) is replaced over time by its labeled counterpart, and the fraction of unlabeled X (X^U/X^T, where X^T is the intracellular concentration) will decay over time. The rate of this decay is determined by the ratio of the flux through X (f_X) to the total pool size of X (X^T). Therefore, the flux through X (f_X) can be calculated from this rate of decay and the intracellular pool size (43).

We constructed an ordinary differential equation (ODE) model for the metabolic network shown in Fig. S10 in the supplemental material and then identified model parameters (fluxes and oxaloacetate pool size) that reproduce the laboratory data. The procedure was based on methods previously developed (2, 16, 35). The ODEs described the rates of loss of unlabeled forms of metabolites (and the creation of particular labeled forms) after feeding of [U-^{13}C]glucose. The equations are based on flux balance of metabolites and take the form of:

$$\frac{dB}{dt} = \sum_{i=1}^{N} F_i \frac{A_i}{A_{tot}} - F_{tot} \frac{B}{B_{tot}},$$

where a metabolite B is a specific labeled or unlabeled form of a metabolite that can be produced from other metabolites A_i. The outflux F_{tot} of balances the sum of N influxes F_i from A_i. A_{tot} and B_{tot} are the total pool sizes of the corresponding metabolite (sum of labeled and unlabeled forms).

The unknown model parameters were identified by a genetic algorithm that minimizes a cost function (15, 16). The cost function (see Table S4 in the supplemental material) quantifies the difference between the computational model output and the experimentally observed labeling dynamics. It further enforces agreement with the experimentally observed glucose uptake and acid/solvent production rates (2). With the exception of the oxaloacetate concentration (which could not be determined experimentally), all of the model parameters represent metabolic fluxes. For each laboratory data set (two independent acidogenic and two independent solventogenic cultures), we ran the genetic algorithm 10 separate times, each starting from a random initial point and yielding 100 consistent parameter sets. The parameter distributions generated by these sets are shown in see Fig. S11 in the supplemental material. The median value and the breadth of the distribution provide a representation of the metabolic fluxes that are consistent with the laboratory data. The C/C++ program used for the modeling and parameter identification are available upon request.

RESULTS

Intracellular metabolite levels during the acidogenic-solventogenic transition. The metabolism of *C. acetobutylicum* is characterized by an initial acidogenic phase (exponential growth), followed by solvent production and acid re-assimilation. The goal of the present study was to characterize the metabolic changes associated with the transition from exponential growth to solventogenesis. The system under study consisted of pH-controlled (pH 4.7) batch cultures grown on chemically defined media containing glucose as the sole carbon source and ammonia as the sole nitrogen source. As shown in Fig. 1A, as the culture exits the exponential growth phase, the rate of acid production decreases and solvent production begins. A few hours later, the concentration of acids in the media starts to decrease due to their re-assimilation and conversion into solvents. Cell growth continues during solventogenesis, albeit at a slower rate than during the exponential phase. The

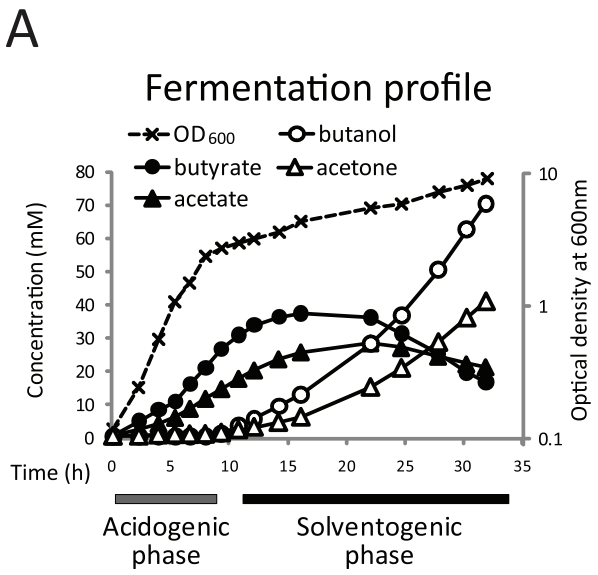

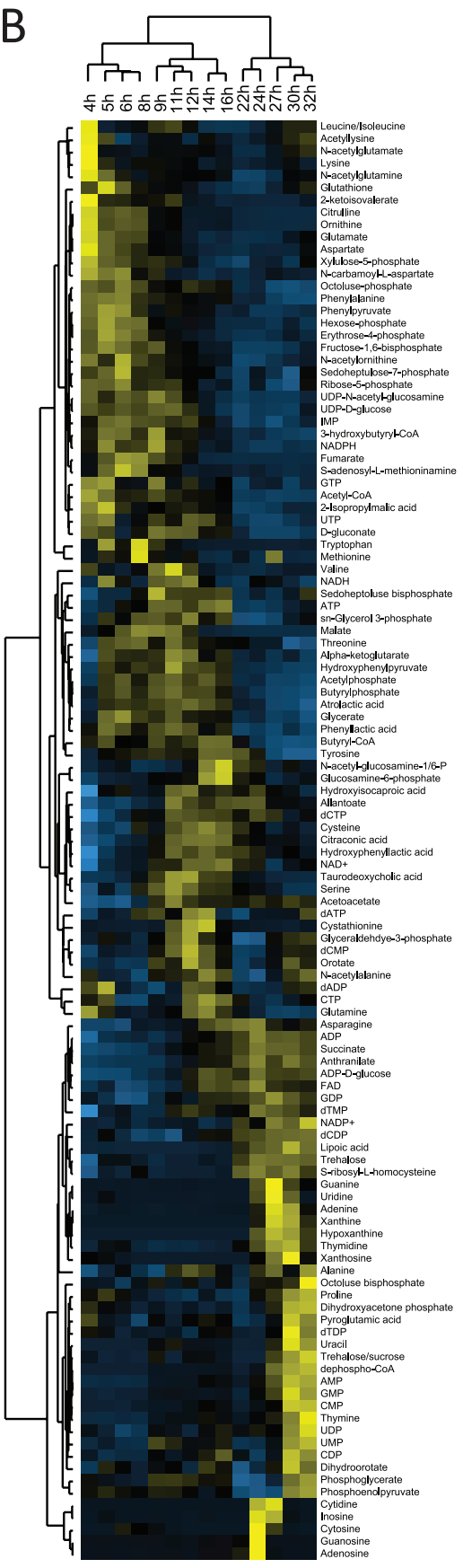

FIG. 1. Progressive metabolome remodeling during the acidogenic-solventogenic transition. (A) Fermentation profile and growth curve obtained in a pH 4.7 controlled batch culture. (B) Metabolome dynamics during the acidogenic-solventogenic transition. Unsupervised hierarchical cluttering analysis of 114 intracellular metabolite levels was perfromed. Rows represent specific intracellular metabolites. Columns correspond to the fermentation time points shown in panel A, starting at 4 h. Relative metabolite concentrations across time points are normalized to have a mean equal to 0 and a standard deviation equal to 1. Metabolites whose levels are higher than the mean across time points are shown in shades of yellow and those with lower levels than the mean in shades of blue. The individual profiles for each metabolite can be found in Fig. S1 in the supplemental material. The data represent the averages of two replicate measurements from a single batch culture and are representative of the results obtained in three independent experiments (see Fig. S2 in the supplemental material). Hexose-phosphate represents the combined pools of glucose-6-phosphate and fructose-6-phosphate. Phosphoglycerate represents the combined pools of glycerate-2-phosphate and glycerate-3-phosphate.

observed fermentation profile is typical for *C. acetobutylicum* batch cultures.

Samples for the analysis of intracellular and extracellular metabolites were taken over a 28-h period (14 time points). The first four data points (4 to 8 h) correspond to mid- to late-acidogenic phase, the remaining time points correspond to the transitional and solventogenic phases (9 to 32 h). Based on its fermentation profile, the solventogenic phase can be divided into two stages: an early solventogenic phase (11 to 16 h) in which mixed acid-solvent production is observed and a mid-solventogenic phase (22 to 32 h) where acid re-assimilation takes place and the rate of solvent production increases. Late solventogenesis, where acid re-assimilation stops and solvent production decreases, was beyond the scope of the present study and was not examined. Samples were analyzed by a set of liquid LC-MS methods which together enable the analysis of ~200 known metabolites. Quantitative data (relative or absolute concentrations) throughout the time course was obtained for 114 intracellular metabolites and 50 extracellular metabolites. Absolute concentrations were obtained for 79 of the intracellular metabolites, and relative concentrations were obtained for 35 intracellular metabolites.

Our analysis revealed an orderly progression of changes in the levels of intracellular metabolites throughout the time course (Fig. 1B and see Fig. S1 and S2 in the supplemental material). Rather than being restricted to metabolites in the acid-solvent-producing pathways, these alterations encompassed all analyzed pathways. The unsupervised hierarchical clustering analysis shown in Fig. 1B highlights the major trends in the data. The time point samples cluster into three major groups corresponding to the exponential (acid production), early solventogenic (mixed acid/solvent production), and mid-solventogenic (acid reutilization with solvent production) phases. This clustering, based solely on the measured metabolite levels, is fully consistent with the actual order of sample collection. While metabolites belonging to the same class (such as amino acids) or pathway (such as glycolysis) do not always cluster together, some general trends are evident: most amino acids, upper glycolytic intermediates, and pentose phosphate pathway compounds are at high levels in acidogenesis and lower levels in solventogenesis; butyryl-phosphate and acetyl-phosphate are at high levels during acidogenesis and early solventogenesis but at low levels in late solventogenesis; ATP, NADH, and butyryl-CoA peak in early solventogenesis; and the levels of low-energy forms of nucleotides (including diphosphates, monophosphates, nucleosides, and bases) increase late in the time course.

Changes in the composition of the core *C. acetobutylicum* metabolome. The absolute intracellular concentrations of 79 metabolites were determined in acidogenic and solventogenic cells (Table 1). The intracellular metabolome was dominated, on a molar basis, by a small number of abundant metabolite classes: amino acids (~55% during both acidogenesis and solventogenesis), central carbon intermediates (~27% during acidogenesis, 17% in solventogenesis), and nucleotides (5% during acidogenesis, 10% in solventogenesis). Similar to *E. coli* (6), during exponential growth the most abundant metabolites were glutamate and fructose-1,6-bisphosphate.

The transition from exponential growth into solventogenesis has significant effects on the overall metabolome composition (Fig. 2A). We observed a decrease in the total concentration of measured metabolites, from ~150 mM during the mid-exponential phase to ~70 mM during mid-solventogenesis. This reflects in large part decreases in concentration of a few highly abundant metabolites such as glutamate, which is both a key nitrogen donor and a counter ion for potassium. Glutamate is replaced in part by aliphatic amino acids, transiently by valine, and subsequently by alanine. Fructose-1,6-bisphosphate, the second most abundant metabolite during exponential growth, also declines steadily during the transition to solventogenesis.

In the nucleotide class, the ratio of high-energy triphosphates to lower-energy bisphosphates and monophosphates decreases in solventogenesis (Fig. 2B). In *C. acetobutylicum*, a major route of ATP generation is acid production. Conversely, a main route for acid re-assimilation utilizes ATP. Therefore, the switch from acid production to acid re-assimilation may cause the observed decrease in energy charge.

The ratio of redox cofactors is also affected. Surprisingly, both the NADH/NAD^+ the and NADPH/$NADP^+$ ratios decrease during solventogenesis (Fig. 2C). This may initially appear counterintuitive since high NAD(P)H/$NAD(P)^+$ ratios

TABLE 1. Intracellular metabolite concentrations in acidogenesis and solventogenesis[a]

Metabolite	Concn (mM)	
	Acidogenic	Solventogenic
Acetyl-CoA	1.6736	0.4575
Acetylphosphate	0.6337	0.3195
ADP	0.8190	0.6683
ADP-glucose	0.0004	1.4993
AKG	0.2229	0.1375
Alanine	10.0005	6.2890
AMP	0.2988	0.4419
Anthranilate	0.0063	0.0774
Arginine	0.3120	0.5702
Asparagine	0.0353	0.4925
Aspartate	7.0482	1.1698
ATP	3.2656	0.9530
Butyryl-CoA	1.8968	0.6180
Citrate	0.0004	0.0002
Citrulline	8.6691	0.6283
CMP	0.0964	0.1656
CTP	0.4898	0.2032
dADP	0.0202	0.0831
dATP	0.0725	0.0785
dCDP	0.0045	0.0149
dCMP	0.0070	0.0024
dCTP	0.1392	0.0472
DHAP	1.0638	0.2513
dTMP	0.0037	0.0113
Erythrose-4-phosphate	0.8920	0.1715
FAD	0.6438	0.3805
FBP	21.9042	2.4186
Fumarate	0.8219	0.0586
Hexose-phosphate	6.7361	1.1526
GAP	0.3142	0.1500
GDP	0.0449	0.2234
Gluconic acid	0.0421	0.0200
Glutamate	26.6743	3.2572
Glutamine	8.7740	2.0087
Glutathione	0.1069	0.0120
Phosphoglycerate	5.4727	1.0071
Glycine	4.8549	0.7834
GMP	0.0606	0.0624
GTP	1.5583	0.8563
Histidine	0.0802	0.0427
3-Hydroxybutyryl-CoA	0.0706	0.0196
Hydroxyisocaproic acid	1.2256	1.3220
Hydroxyphenylpyruvate	0.4148	0.1752
IMP	0.4297	0.0583
2-Keto-isovalerate	1.8267	0.1463
Leucine/isoleucine	0.6304	0.1457
Lysine	1.3066	1.0608
Malate	0.0797	0.0251
Malonyl-CoA	0.0202	0.0019
Methionine	0.2485	0.0464
N-Acetylalanine	0.0259	0.0154
N-Acetylglucosamine	0.3452	0.3643
N-Acetylglucosamine-1,6-phosphate	0.1121	0.1183
N-Acetylglutamine	1.2787	0.2690
N-Acetylornithine	0.6135	0.0680
NAD^+	1.6046	1.2327
NADH	0.3393	0.1228
$NADP^+$	0.0042	0.0024
NADPH	0.2415	0.0177
Ornithine	1.4594	0.3150
Phosphoenolpyruvate	1.2593	0.1687
Phenylalanine	0.1420	0.0711
Phenylpyruvate	0.0610	0.0025
Proline	1.2303	0.1908
Ribose-5-phosphate	0.1646	0.0504
Sedoheptulose-1/7-phosphate	0.3282	0.1252
Serine	0.5568	0.8617
sn-Glycerol-3-phosphate	0.8427	0.3445
Threonine	6.2009	2.3949
Thymidine	0.0369	0.1237
Tryptophan	0.1948	0.0814
Tyrosine	0.6592	0.6404
UDP	0.0625	0.0577
UDP-glucose	3.2497	0.9148
UDP-*N*-acetylglucosamine	1.0992	0.4161
UMP	0.0247	0.0242
UTP	1.3446	0.3086
Valine	9.8207	0.9305
Xylulose-phosphate	0.4136	0.0957

[a] Concentration values correspond to mid-exponential-phase growth (t = ~5 h) and mid-solventogenesis (t = ~22 h).

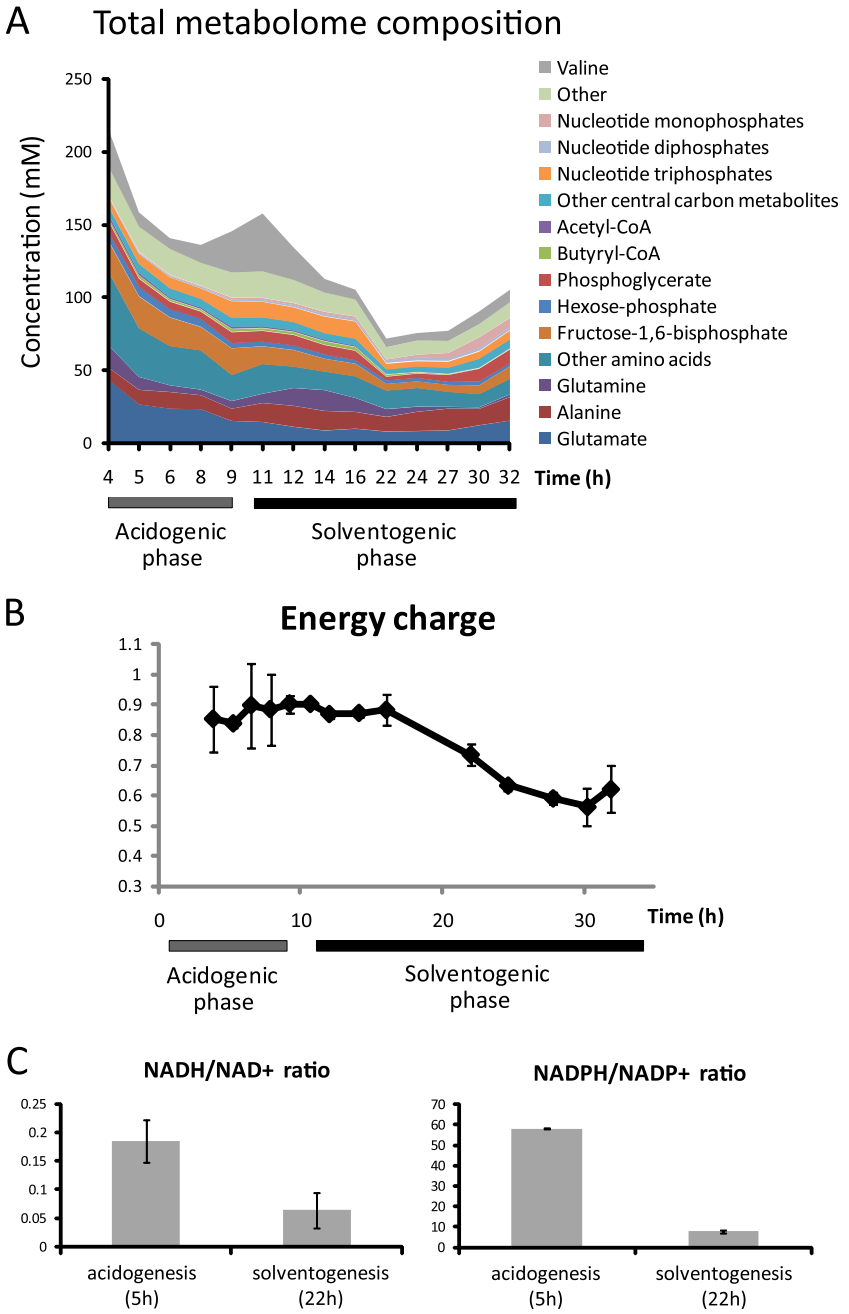

FIG. 2. Changes in metabolome composition, energy charge, and NAD(P)H/NAD(P)$^+$ ratios during acidogenic-solventogenic transition. (A) Changes in overall metabolome composition. The graph shows the molar abundance of 79 different metabolites, most of them combined as groups of metabolites, during acidogenic-solventogenic transition. The metabolite data and time points correspond to the fermentation shown in Fig. 1A. The data shown represents the average of two replicate measurements from a single batch culture and are representative of three independent experiments (see Fig. S2 in the supplemental material). Hexose-phosphate represents the combined pools of glucose-6-phosphate and fructose-6-phosphate. Phosphoglycerate represents the combined pools of glycerate-2-phosphate and glycerate-3-phosphate. (B) Energy charge during the acidogenic-solventogenic transition. The energy charge (E) was calculated as follows: $E = ([ATP] + 1/2[ADP])/([ATP] + [ADP] + [AMP])$. The metabolite data and time points correspond to the fermentation shown in Fig. 1A. The error bars show ± the standard errors. (C) NADH/NAD$^+$ and NADPH/NADP$^+$ ratios during acidogenesis and solventogenesis. The data represent the averages of two replicate measurements from two independent experiments. The error bars show ± the standard errors.

should favor solvent production. However, the decrease in these ratios may result from rapid consumption of NADH and NADPH by solvent-producing pathways. It has been shown that high NADH/NAD ratios reduce the activity of glyceraldehyde-3-phosphate dehydrogenase (GAPDH) in *C. acetobutylicum* (17). A potential benefit of maintaining a low NADH/NAD ratio during solventogenesis would be to maintain glycolytic flux; if this ratio were to be increased in order to drive solventogenesis, it could potentially have an adverse effect on glycolytic flux because of the inhibition of GAPDH.

Extracellular metabolites. In addition to the typical fermentation products (i.e., acetate, butyrate, butanol, ethanol, and acetone), we detected and quantified 50 extracellular metabolites (Fig. 3A and see Fig. S3 in the supplemental material). During exponential growth, modest amounts of malate, fumarate, succinate, and pyruvate are secreted into the media (Fig. 3C). As the cells exit exponential phase, malate and fumarate are rapidly consumed. Succinate excretion continues during early solventogenesis but slows markedly during mid-solventogenesis.

At the onset of solvent production, a large number of typically intracellular metabolites, including phosphorylated compounds, start to accumulate in the media (Fig. 3A). The total concentration of extracellular metabolites increases from ~1 mM during acidogenesis to ~3 mM during solventogenesis (Fig. 3B). One possible explanation is increased membrane permeability during solventogenesis caused by the accumulation of extracellular butanol, which may have a chaotropic effect that disrupts the integrity of the cellular membrane. In *C. acetobutylicum*, butanol has been shown to affect membrane fluidity and composition, generally increasing the ratio of saturated to unsaturated fatty acids tails in membrane phospholipids (3, 4, 29, 39, 41). However, some metabolites with large intracellular concentrations, such as glutamate or glutamine, are not detected extracellularly at significant levels during solventogenesis. It is possible that active uptake mechanisms exist for potentially useful metabolites such as this (glutamate and glutamine are valuable carbon and nitrogen sources) that prevent them from accumulating extracellularly despite some leakage caused by increased membrane permeability during solventogenesis.

Metabolic impact of pH, acids, and solvents. As the cells transition from acidogenesis into solventogenesis, they are subjected to several changes in their environment: acid accumulation, decreasing pH, increasing cell density, and finally solvent accumulation. Here we examined the metabolic consequences of maintaining the fermentation culture at pH 6.0, of adding exogenous acid, or of adding exogenous butanol. As expected based on prior literature (33), maintaining the fermentation at pH 6 increased initial cell growth and allowed only a very short period of solvent production as the cells exit exponential growth (see Fig. S4A in the supplemental material). There was no acid reuptake or overt solventogenic phase. Consistent with these observations, the metabolome pattern during acidogenesis and up to the onset of solventogenesis was largely unaffected but then diverged markedly from the lower pH culture (see Fig. S4B in the supplemental material).

To test the effects of acid accumulation, together with a drop in pH, we added exogenous butyrate (30 mM) and acetate (30 mM) to exponentially growing cells (OD_{600} = 0.6, initial pH 6.0) while simultaneously decreasing the pH to 4.7. This treatment did not, on a short time scale (2 h), trigger solvent production and did not reproduce the overall metabolic changes observed during acidogenesis or early solventogenesis (see Fig. S6A in the supplemental material). However, the addition of acids caused a large increase in the levels of butyryl-CoA, butyryl-phosphate, and acetyl-phosphate and a modest transient increase in acetyl-CoA levels (see Fig. S6B in the supplemental material). This suggests that the extracellular accumulation of acids during acidogenesis and early solventogenesis may be responsible for the increase in the levels of some of these metabolites during that time. The inability of this treatment to initiate the transition into solventogenesis suggests that other factors, perhaps related to high cell densities, are also required to produce the full scope of metabolic changes leading to effective solventogenesis.

To test whether butanol is responsible for the increased membrane permeability or metabolome changes during solventogenesis, we treated exponentially growing cells (OD_{600} = 0.6, pH controlled at 6.0) with butanol (70 mM). We observed a decrease in growth rate of ca. 30% after butanol addition. There was not, however, substantial release of intracellular metabolites into the media (see Fig. S7A in the supplemental material). Although butanol did not have a discernible effect on membrane permeability, it had significant effects on the intracellular concentrations of several metabolites (see Fig. S7B in the supplemental material). These included a rapid increase in valine, leucine/isoleucine, and glutamine that have a slight similarity to the changes occurring at the time of the solventogenic transition. In *B. subtilis*, changes in membrane fluidity can be accomplished by the synthesis of branched-chain fatty acids from the branched amino acids valine, leucine, and isoleucine (32). It has been established that *C. acetobutylicum* adjusts membrane fluidity in response to butanol stress (3, 4, 29, 39, 41) and that branched-chain amino acid biosynthetic genes are upregulated at the onset of solvent production (1, 26). Therefore, it is likely that the increased production of branched-chain amino acids that we observe at the onset of solventogenesis, and during butanol challenge, enable synthesis of branched-chain fatty acids and adjustments to membrane fluidity. However, with the exception of the few branched-chain amino acids just discussed, the addition of butanol failed to reproduce the intracellular concentration changes associated with the transition into solventogenesis (see Fig. S7 in the supplemental material).

The results of the experiments in this section indicate that no single factor (low pH, acid or solvent accumulation) is responsible for the organized, progressive metabolome evolution during the solventogenic transition; instead, multiple factors are required to drive this progression.

Probing intracellular fluxes. In addition to metabolite concentrations, *in vivo* reaction rates are among the most important characteristics of a biochemical network. The widespread changes in metabolite concentrations during the acidogenic-solventogenic transition suggested that core metabolic fluxes are affected. Although metabolic fluxes are not directly observable, they can be measured based on nutrient uptake and waste excretion rates and on the assimilation of stable isotope tracers into intracellular metabolites.

During solventogenesis the specific rate of glucose consumption decreases >3-fold, going from ~12 mM h^{-1} grams cell dry weight^{-1} ($gCDW^{-1}$) during the mid-exponential phase to ~3.5 mM h^{-1} $gCDW^{-1}$ during the mid-solventogenic phase. About 60 to 70% of the consumed glucose is excreted as acids during acidogenesis. During solventogenesis, as much as 85% of the glucose consumed is converted into solvents while additional solvent production eventually occurs from acid reutilization. The overall conversion yield of glucose to biomass is

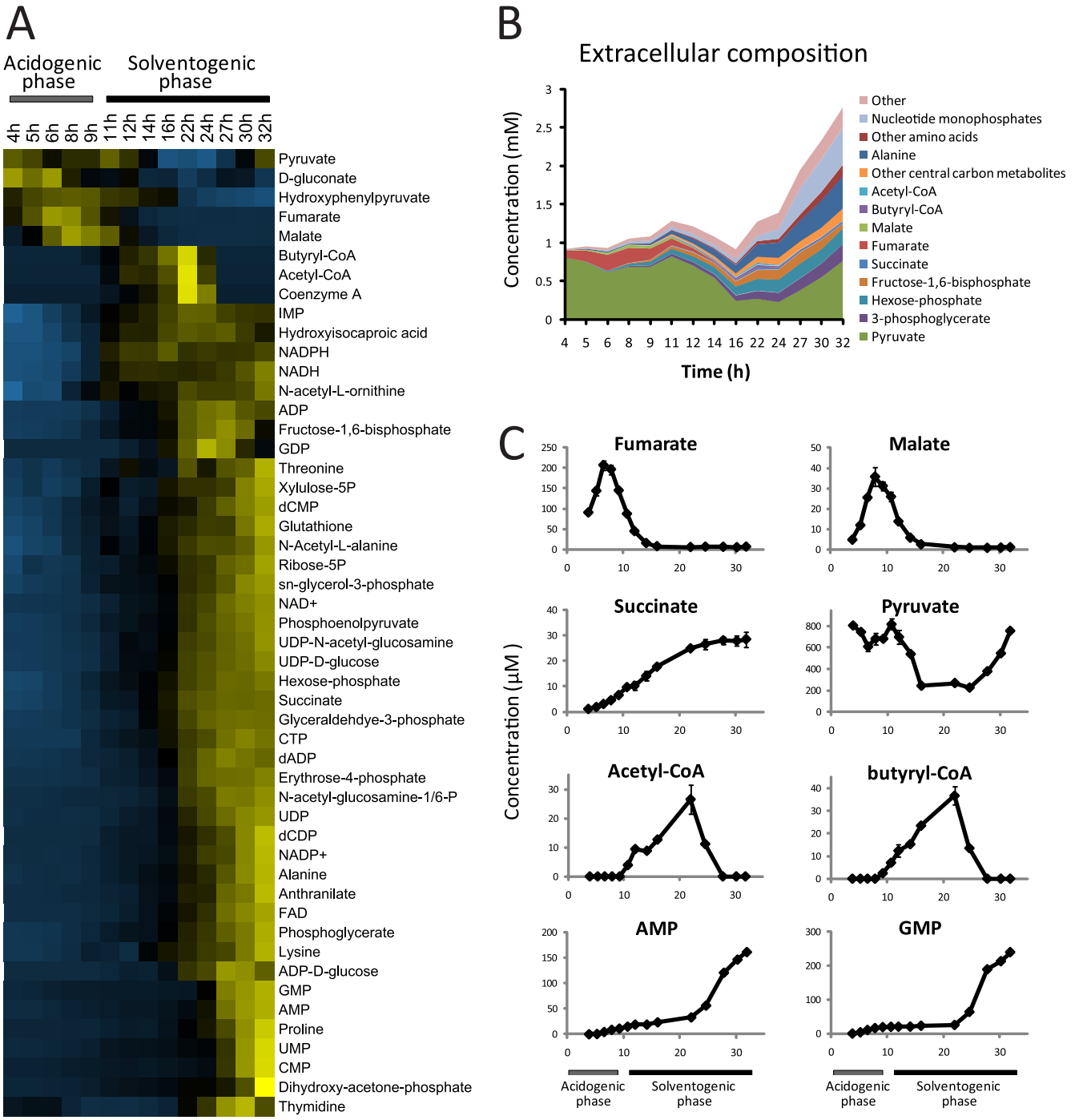

FIG. 3. Extracellular metabolites during the solventogenic transition. (A) Unsupervised hierarchical cluttering analysis of extracellular metabolite concentration data. Rows represent specific metabolites. Columns correspond to the fermentation time points shown in Fig. 1A, starting at 4 h. Metabolite concentrations across time points are normalized to have a mean equal to 0 and a standard deviation equal to 1. Concentrations that are higher than the mean across time points are shown in shades of yellow and those lower than the mean in shades of blue. The concentration data for each metabolite can be found in Table S2 in the supplemental material. The data represent the average of two replicate measurements from a single batch culture and are representative of the results obtained in three independent experiments (see Fig. S3 in the supplemental material). Hexose-phosphate represents the combined pools of glucose-6-phosphate and fructose-6-phosphate. (B) Extracellular metabolome composition. The graph shows the molar abundance of 50 different metabolites, most of them combined as groups of metabolites, during the acidogenic-solventogenic transition. (C) Extracellular concentration profiles of selected metabolites. The concentration data for each metabolite can be found in Table S2 in the supplemental material. The error bars show ± the standard errors.

higher during acidogenesis (~31 gCDW mol^{-1}) than during solventogenesis (~17 gCDW mol^{-1}).

Since glucose consumption decreases during solventogenesis, overall intracellular metabolic flux must also decrease. However, we do not expect all metabolic pathways to be equally (proportionally) affected. To investigate the remodeling of central metabolic fluxes during solventogenesis, we monitored the dynamics of incorporation of labeled glucose into intracellular metabolites during acidogenesis and solventogenesis. Universally ^{13}C-labeled glucose was added into mid-exponential or mid-solventogenic cultures in a matching amount to the nonlabeled glucose remaining in the media to reach a 1:1 ratio between ^{13}C-labeled and nonlabeled glucose. Samples were taken at short time intervals (e.g., 1, 2, 3, 5, 7, 10, 15, 30, and 60 min) after [^{13}C]glucose addition. The rate of incorporation of ^{13}C-labeled glucose into downstream metabolites was monitored using LC-MS.

Consistent with the persistent uptake of glucose throughout the fermentation, the rate of incorporation of ^{13}C-labeled glucose into glycolytic intermediates (e.g., hexose-phosphates, fructose-1,6-bisphosphate, dihydroxyacetone-phosphate, and phosphoenolpyruvate) and pentose phosphate pathway metabolites (e.g., ribose-5-phosphate) is fast in both acidogenic and solventogenic cells (Fig. 4). By 1 min, metabolites in these pathways reach isotopic steady state (no further change in their ^{13}C-labeled fraction). The steady-state labeling fraction of these metabolites is consistent with the ~50% labeling of extracellular glucose. In contrast, the labeling rate in most amino acids is considerably slower during solventogenesis compared to acidogenesis. In the reductive TCA cycle, malate and fumarate display nearly nondetectable labeling during solventogenesis. However, metabolites in the oxidative TCA cycle, such as citrate, still become labeled.

Several acidogenic/solventogenic metabolites display interesting labeling patterns. Although the labeling rate of acetyl-CoA is comparable to glycolytic intermediates, it does not reach the expected 50% ^{13}C-labeled fraction in either acidogenic (only 35%) or solventogenic (only ~25%) cells (Fig. 4). The ^{13}C-labeled fraction in acetyl-phosphate is even lower: ~10% in acidogenic and ~5% in solventogenic cells. These labeling patterns are expected in solventogenic cells where nonlabeled acetate is re-assimilated from the media and converted into acetyl-phosphate and acetyl-CoA, but not in acidogenic cells with high rates of acetate production. The lower-than-expected ^{13}C-labeled fraction of acetyl-CoA and acetyl-phosphate suggests that, even during acidogenesis, there is a rapid interchange between the acetyl-CoA pool and the extracellular acetate pool, likely achieved through the rapid reversibility of the enzymes phosphotransacetylase (conversion of acetyl-CoA to acetyl-phosphate) and acetate kinase (conversion of acetyl-phosphate to acetate). Consistent with this hypothesis, when we added ^{13}C-labeled acetate to acidogenic cultures, we observed rapid labeling of intracellular acetyl-phosphate, followed by partial labeling of acetyl-CoA and downstream metabolites such as butyryl-CoA (see Fig. S8A in the supplemental material). In addition, using a filter culture methodology (2, 42), acidogenic cells can be rapidly switched to fresh media containing 100% ^{13}C-labeled glucose with no extracellular acetate. In this situation, rapid and complete labeling of acetyl-CoA and acetyl-phosphate are observed (butyryl-CoA and butyryl-phosphate are also rapidly and completely labeled), indicating that partial labeling of acetyl-CoA and acetyl-phosphate in batch fermentation experiments is due to extracellular unlabeled acetate (see Fig. S8B in the supplemental material). Similarly to acetyl-CoA and acetyl-phosphate, butyryl-CoA and butyryl-phosphate do not reach their expected ^{13}C-labeled fractions in acidogenic cells. This also suggests a rapid interchange also between butyryl-CoA and extracellular nonlabeled butyrate. Finally, the hypothesis of a rapid interchange between extracellular acids and their intracellular CoA derivatives also implies that, as the fractions of extracellular ^{13}C-labeled acetate and butyrate slowly increase in the media after the addition of [^{13}C]glucose, the ^{13}C-labeled fractions of acetyl-CoA, butyryl-CoA, acetyl-phosphate, and butyryl-phosphate will also slowly increase beyond the initial pseudo-steady-state values discussed above. Figure S8C in the supplemental material shows this phenomenon at longer time scales (1 h).

It has been previously established that *C. acetobutylicum* has a bifurcated TCA cycle: oxaloacetate flows to succinate both through citrate/α-ketoglutarate (oxidative branch) and via malate/fumarate (reductive branch) (2, 11). We argued that such a bifurcated TCA cycle could play a role in cellular redox balance (2). Here we find that during solventogenesis the electron-consuming reductive TCA cycle is shut down, since there is no detectable labeling of malate or fumarate from ^{13}C-labeled glucose (Fig. 4). However, the NADH producing oxidative (clockwise) right side of the TCA cycle remains active. This reorganization may represent a deliberate effort to channel reducing power toward solvent production. As shown before, malate and fumarate are excreted during acidogenesis and re-assimilated during the transition into solventogenesis (Fig. 3C). To determine the fate of the re-assimilated fumarate, we added ^{13}C-labeled fumarate during the time of the acidogenic-solventogenic transition. The labeled fumarate was rapidly converted to malate and metabolized via the TCA cycle into glutamate or aspartate (see Fig. S9 in the supplemental material). This rapid re-assimilation of fumarate and malate during the transition may be helpful in kick-starting or sustaining early solvent production by providing additional reducing power.

It is possible that the switch into solventogenic metabolism involves not only changes in metabolic fluxes but the utilization of alternative pathways in core metabolism. In particular, the oxidative pentose pathway or the Entner-Doudoroff pathway for glucose catabolism could be advantageous for the production of NADPH. Previously, we ruled out the activity of these pathways during acidogenesis using additional labeled substrates such as [1,2-^{13}C]glucose (2). Similar experiments conducted here show that during solventogenesis these pathways are also not active. In addition, the correspondence between the amino acid labeling patterns of acidogenic and solventogenic cells indicates that the routes for amino acid biosynthesis also remain unchanged (see Table S3 in the supplemental material).

Quantitative flux analysis during acidogenesis and solventogenesis. We used kinetic flux profiling (KFP) (42) to obtain a quantitative estimate of metabolic fluxes from the kinetics of incorporation of ^{13}C-labeled glucose into downstream metabolites during acidogenesis and solventogenesis. We con-

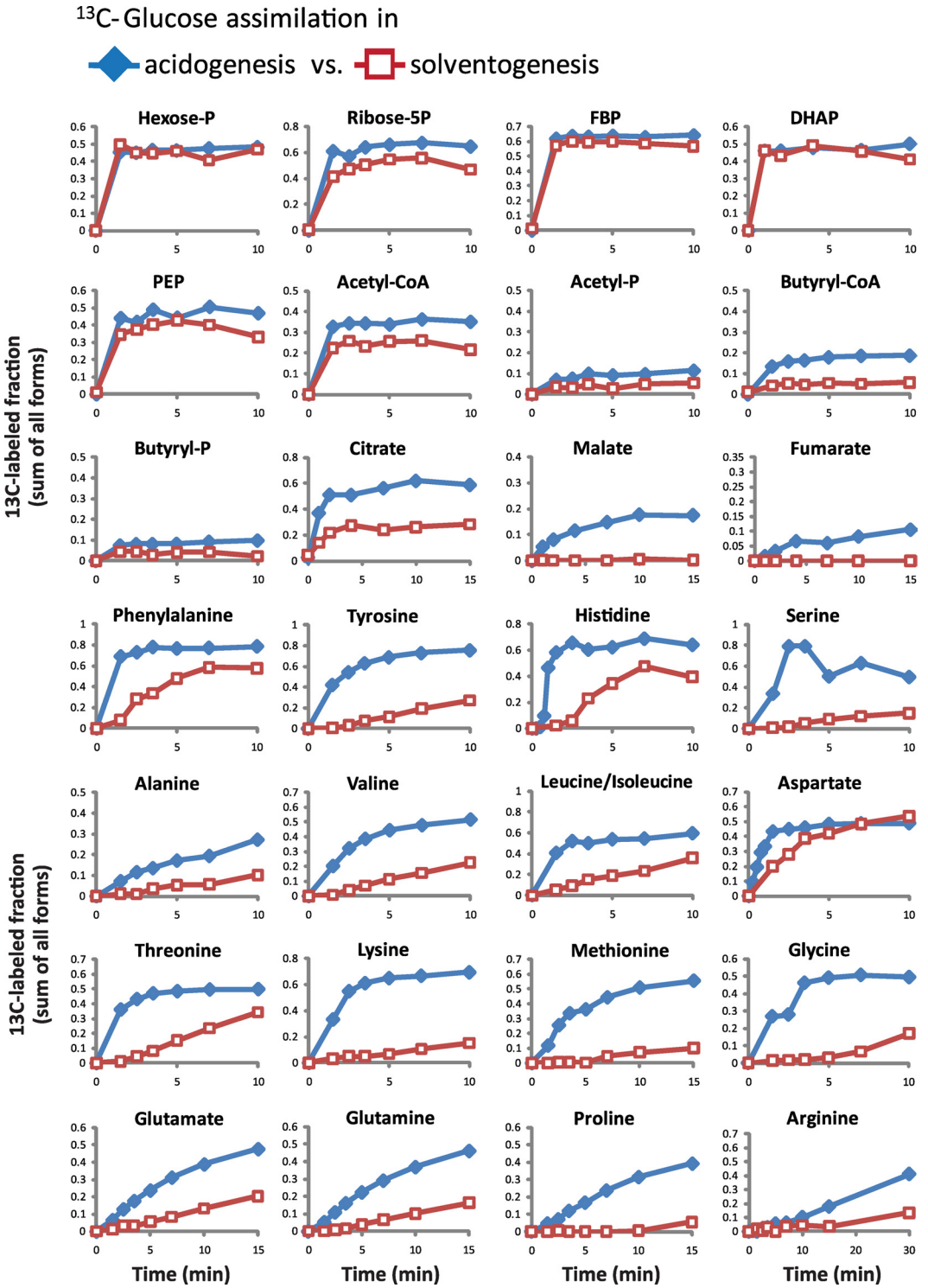

FIG. 4. Isotopic tracer experiments reveals differences in pathway activity in acidogenic versus solventogenic cultures. The rate of incorporation of ^{13}C-labeled glucose into downstream metabolites reveals differences in pathway activity in acidogenic versus solventogenic cultures. At time = 0, universally ^{13}C-labeled glucose was added into mid-exponential-phase or mid-solventogenic-phase cultures in a matching amount to the nonlabeled glucose remaining in the media to reach a 1:1 ratio between ^{13}C-labeled and nonlabeled glucose. Samples were taken at short time intervals after [^{13}C]glucose addition, and the incorporation of ^{13}C-labeled glucose into downstream metabolites was monitored using LC-MS. The line graphs represent the ^{13}C-labeled fraction (sum of all different labeled forms) of the indicated metabolite as a function of time. The data shown are one data set representative of two independent acidogenic and two independent solventogenic cultures. The complete data set is included in Table S3 in the supplemental material.

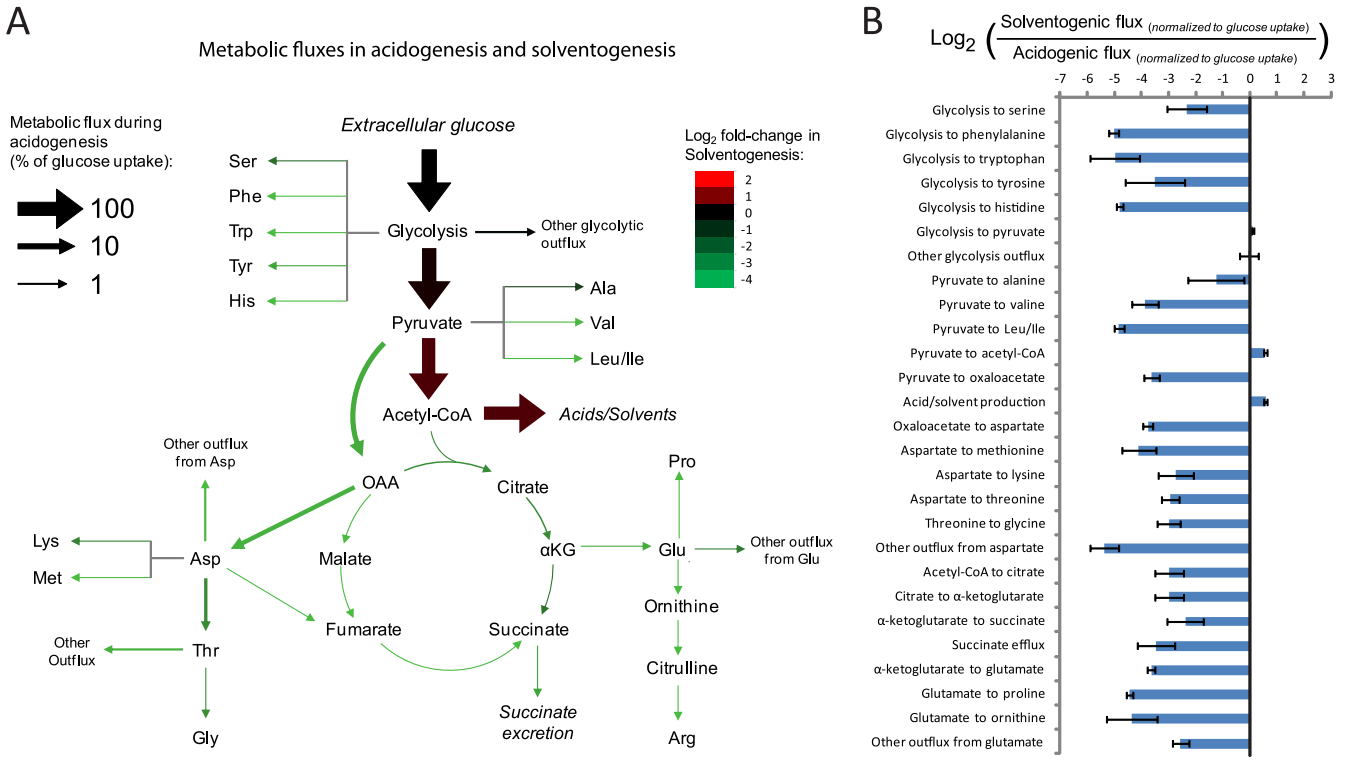

FIG. 5. Alterations in metabolic fluxes during solventogenesis. We used kinetic flux profiling (KFP) to obtain a quantitative estimate of metabolic fluxes from the kinetics of incorporation of ^{13}C-labeled glucose into downstream metabolites during acidogenesis and solventogenesis. We constructed an ordinary differential equation (ODE) model for the metabolic network shown in Fig. S10 in the supplemental material. One-thousand sets of fluxes (unknown model parameters) that can reproduce the experimental labeling dynamics were identified using a genetic algorithm. (A) Averages of the median flux values (normalized to glucose uptake) obtained from two independent acidogenic cultures. (B) Fold change in median flux values during solventogenesis. The fold change is calculated as the $\log_2(\text{flux}_S/\text{flux}_A)$, where flux_S is the solventogenic flux normalized to the glucose uptake and flux_A is the acidogenic flux normalized to the glucose uptake. Data from two independent acidogenic and two independent solventogenic cultures were used in these calculations (see Table S3 in the supplemental material). The mean flux values obtained from each of these experiments are shown in Table S5 in the supplemental material. The one-thousand individual set of fluxes for all cultures are included in Table S6 in the supplemental material, and their distributions are shown in Fig. S11 in the supplemental material. During solventogenesis, the incorporation of ^{13}C-labeled glucose into malate and fumarate is negligible (Fig. 4); therefore, the fold changes for these fluxes are omitted from this figure. The error bars show ± the standard errors.

structed an ordinary differential equation (ODE) model for the metabolic network shown in Fig. S10 in the supplemental material that describes the isotope labeling kinetics of metabolites following the addition of universally labeled [^{13}C]glucose. Given the model equations, we used a nonlinear global search algorithm (genetic algorithm) to identify sets of fluxes that can quantitatively reproduce the experimental labeling dynamics (16). The inputs to the model included the metabolite labeling kinetics, intracellular metabolite concentrations, glucose uptake rate, and acid/solvent production rates.

Figure 5 shows a map of the identified median flux values (normalized to glucose consumption) during acidogenesis (Fig. 5A) and their fold changes during solventogenesis (Fig. 5B). Although glycolytic flux during solventogenesis decreases proportionally to the specific rate of glucose consumption, we observed a disproportionally large decrease in the synthesis of nearly all amino acids. After normalizing to glucose uptake, the average decrease of carbon flux into amino acids during solventogenesis is ~14-fold. This large and generalized decrease in amino acid biosynthesis redirects carbon toward acetyl-CoA and the acidogenic/solventogenic pathways (Fig. 5B). Amino acid biosynthesis requires large amounts of ATP and NADPH. Therefore, the decrease in amino acid biosynthesis during solventogenesis means that limited energy and reducing power can be instead directed toward solvent production. Indeed, the fact that the energy charge and the NADPH/NADP$^+$ ratio decrease during solventogenesis suggests that ATP and/or NADPH may be limiting resources during solventogenesis. As mentioned before, we observed a spike in the concentration of some amino acids (serine and valine) during the transition and early solventogenesis; at this time, however, the energy charge and NADPH/NADP ratio are still relatively high.

Our results suggest that the regulation of metabolic fluxes surrounding pyruvate is a hallmark of the transition into solventogenic metabolism. The various alterations that we observe have the net effect of redirecting flux from pyruvate into acetyl-CoA. Our model estimates a >10-fold decrease of carbon flux into oxaloacetate from pyruvate (catalyzed by pyruvate carboxylase), which appears to be of particular importance since this is the second largest outflux from pyruvate during acidogenesis (Fig. 5A). Since oxaloacetate is required as a precursor for the biosynthesis of 11 different amino acids, reduced flux through pyruvate carboxylase may be a major

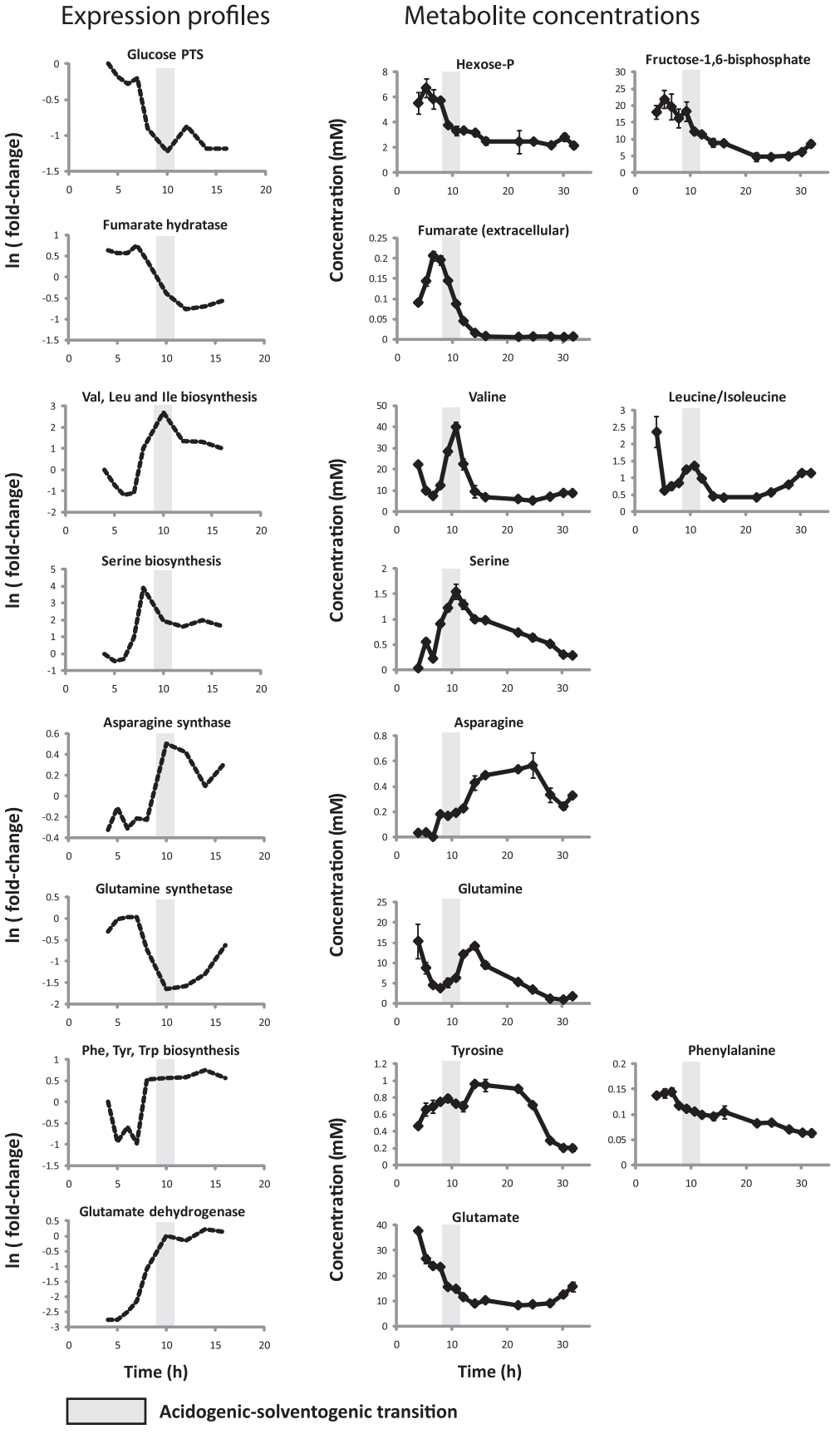
Expression profiles
Metabolite concentrations
Glucose PTS
Hexose-P
Fructose-1,6-bisphosphate
Fumarate hydratase
Fumarate (extracellular)
Val, Leu and Ile biosynthesis
Valine
Leucine/Isoleucine
Serine biosynthesis
Serine
Asparagine synthase
Asparagine
Glutamine synthetase
Glutamine
Phe, Tyr, Trp biosynthesis
Tyrosine
Phenylalanine
Glutamate dehydrogenase
Glutamate
ln (fold-change)
Concentration (mM)
Time (h)
Acidogenic-solventogenic transition

contributing factor in the generalized decrease of amino acid biosynthesis during solventogenesis.

Correlation with transcriptomic studies. Two previous studies have investigated the transcriptional alterations associated with the acidogenic-solventogenic transition in *C. acetobutylicum* (1, 24). The study by Alsaker and Papoutsakis reported the changes in gene expression that occur from mid-exponential phase to early solventogenic phase in a pH-controlled batch culture using experimental conditions similar to the ones used in the present study (1). These researchers observed that, in addition to the expected upregulation of solvent-producing genes, the expression of core metabolism genes (i.e., glycolysis, TCA cycle, and amino acid biosynthesis) was significantly affected during the solventogenic transition. We compared the reported gene expression data to our metabolomic data (Fig. 6).

Although the expression of glycolytic genes changes only slightly, glucose-specific phosphotransferase system (PTS) genes were greatly downregulated at the onset of solventogenesis. The expression profile of glucose PTS genes (*cac0570*, *cac2995*, and *cac3427*) correlates with the drop in the levels of the upper glycolysis intermediates hexose-phosphate (combined pools of glucose-6-phosphate and fructose-6-phosphate) and fructose-1,6-bisphosphate (Fig. 6). The PTS system is the main route for glucose uptake in *C. acetobutylicum* (12, 22), and its downregulation and the concomitant low levels of upper glycolysis intermediates may contribute to the decreased glucose uptake and glycolytic flux during solventogenesis. Moreover, the PTS system consumes phosphoenolpyruvate, providing one of the major drains from the bottom of glycolysis. Decreased PTS activity is accordingly a potential contributor also to the accumulation of lower glycolytic intermediates during solventogenesis. The other major drain from phosphoenolpyruvate is pyruvate kinase. Given that fructose-1,6-bisphosphate is an allosteric activator of pyruvate kinase in many organisms, its lower levels, also potentially secondary to lower PTS activity, may augment these effects.

We found that the reductive TCA cycle shut downs during solventogenesis and that fumarate levels peak before the onset of solventogenesis. These observations correlate with the decreased expression during the transition of fumarate hydratase (*cac3090* and *cac3091*), which interconverts malate and fumarate. This may be a contributing factor, in addition to lower NAD(P)H levels, to the decreased activity of the reductive TCA.

The majority of ribosomal genes are greatly downregulated at the onset of solventogenesis (1); this implies decreased protein biosynthesis, which is consistent with our observation of the generalized decrease in amino acid biosynthesis. The expression patterns of amino acid biosynthetic genes, however, are more complex (1, 26). Serine, valine, leucine, and isoleucine biosynthetic pathway genes are sharply upregulated during the transition, and their metabolite levels also peak during that time (Fig. 6). The expression levels of other amino acid biosynthetic genes, such as those involved in glutamate, phenylalanine, arginine, and histidine biosynthesis, also increase during solventogenesis (1, 26); however, the associated pathway fluxes and end product concentrations are both markedly decreased. Similarly, the expression of the pyruvate carboxylase gene (*cac2660*) actually increases during solventogenesis, despite the greatly decreased pyruvate carboxylase flux. The reason for high expression of pyruvate carboxylase and certain amino acid biosynthetic genes, whose associated pathways are not metabolically active, is currently unknown. These contradictory findings, however, illustrate the importance of directly measuring metabolic activity rather than merely inferring it from gene expression studies.

DISCUSSION

Our metabolomic studies of the acidogenic-solventogenic transition have provided insights into how *C. acetobutylicum*'s central metabolism is remodeled during solventogenesis. An ordered series of changes in intracellular metabolite concentration occurs as the fermentation progresses from acidogenesis to solventogenesis. These alterations required the dropping pH typical of a *C. acetobutylicum* fermentation. They could not be triggered solely by exogenous acid or solvent addition. The changes were not restricted to the acidogenic/solventogenic pathways but encompass all core metabolic pathways examined. During solventogenesis flux through some of these core pathways, especially pyruvate carboxylase, the reductive branch of the TCA cycle, and amino acid biosynthesis, is greatly reduced. The overall effect of this metabolic remodeling is to redirect resources (carbon, energy, and reducing power) from biomass production into solvent production.

A few previous studies have investigated the changes in intracellular concentrations of selected metabolites during the acidogenic-solventogenic transition. Our observations are generally in good agreement with these previous reports. Using *in situ* fluorescence to measure intracellular NAD(P)H, it has been observed that NAD(H)P levels drop at the onset of solvent production and that NAD(P)H levels and the rate of solvent production have an inverse relationship (37). This agrees with our observations that the NAD(P)H/NAD(P)$^+$ ratios decrease during solventogenesis. Another study looked at the intracellular concentrations of coenzyme A compounds. As we have observed, it was reported that during the shift from the acidogenic to the solventogenic phase, the concentration of butyryl-CoA increased but the concentration of acetyl-CoA decreased (9). Also in agreement with our results, it has been observed that the intracellular concentration of butyryl-phos-

FIG. 6. Correlation between metabolomic data and previous transcriptomic studies. Selected average expression profiles for various enzymes and metabolic pathways are shown on the left. The concentration profiles of related metabolites are shown on the right. The genes used in each average expression profile included the following: glucose phosphotransferase system (PTS), *cac0570*, *cac2995*, and *cac3427*; fumarate hydratase, *cac3091*; valine (Val), leucine (Leu), and isoleucine (Ile) biosynthesis, *cac3173*, *cac3172*, *cac3169*, *cac3176*, *cac0091*, *cac3170*, *cac1479*, *cac0273*, *cac3174*, and *cac3171*; serine biosynthesis, *cac0014*, *cac0015*, and *cac0263*; asparagine synthase, *cac2243*; glutamine synthetase, *cac2658*; phenylalanine, tyrosine, and tryptophan biosynthesis, *cac3162*, *cac3163*, *cac3161*, *cac3159*, *cac3162*, *cac3163*; and glutamate dehydrogenase, *cac0737*. The gray bars indicate the time of the acidogenic-solventogenic transition. Gene expression data were obtained from an earlier study (1).

phate is high during exponential phase and peaks at the onset of solvent production (44). Butyryl-phosphate and acetyl-phosphate were previously reported to have a second delayed peak during late solventogenesis corresponding to acid reutilization, but we did not observe this (44).

Questions regarding cause and effect of the diverse metabolic alterations during the acidogenic-solventogenic transition still remain. Which changes are the primary drivers of solventogenesis? Which are simply by-products of it? For example, we have suggested that decreased amino acid biosynthesis may be an active effort to preserve ATP and NADPH; however, it could also be a by-product of low ATP and NADPH availability caused by decreased acid production and the activation of solvent-producing pathways. The use of genetic engineering approaches to mimic some of the metabolic changes that we observed during solventogenesis, such as elimination of the reductive TCA cycle or decreased amino acid biosynthesis, could help establish causation. In this regard, modulating the activity of pyruvate carboxylase (which converts pyruvate into oxaloacetate) appears to be particularly promising. By redirecting flux into acetyl-CoA and away from oxaloacetate, the downregulation of this enzyme can potentially induce: (i) a generalized decrease in amino acid biosynthesis (oxaloacetate is a precursor for 11 amino acids, including aspartate), (ii) a generalized decrease in nucleotide biosynthesis (aspartate is required for purine and pyrimidine biosynthesis), and (iii) a decrease of flux into the reductive TCA cycle. The observed disconnect between pyruvate carboxylase transcription and activity, however, indicates the likely importance of multiple forms of regulation to engineering efforts.

There have been substantial efforts over the past decade to enhance solvent production in *C. acetobutylicum* by genetic engineering (18, 21, 25). However, these efforts have concentrated almost exclusively on the genes directly involved in the acidogenic-solventogenic pathways. The notion that remodeling of central metabolism plays a causative role in inducing solventogenesis has not yet been explored. A potentially useful approach would be to combine previously described engineered strains with enhanced solventogenesis (such as the acetoacetate decarboxylase [25] and butyrate kinase [20] knockouts) with manipulations that mimic the central metabolic changes that we have observed during solventogenesis. Such a strategy may lead to synergistic (i.e., multiplicative) benefits, by enhancing both acetyl-CoA production and the fraction of acetyl-CoA converted into solvents.

ACKNOWLEDGMENT

This work was funded by grant DE-FG02-07ER64488 from the United States Department of Energy (DOE).

REFERENCES

1. **Alsaker, K. V., and E. T. Papoutsakis.** 2005. Transcriptional program of early sporulation and stationary-phase events in *Clostridium acetobutylicum*. J. Bacteriol. **187:**7103–7118.
2. **Amador-Noguez, D., et al.** Systems-level metabolic flux profiling elucidates a complete, bifurcated tricarboxylic acid cycle in *Clostridium acetobutylicum*. J. Bacteriol. **192:**4452–4461.
3. **Baer, S. H., H. P. Blaschek, and T. L. Smith.** 1987. Effect of butanol challenge and temperature on lipid composition and membrane fluidity of butanol-tolerant *Clostridium acetobutylicum*. Appl. Environ. Microbiol. **53:**2854–2861.
4. **Baer, S. H., D. L. Bryant, and H. P. Blaschek.** 1989. Electron spin resonance analysis of the effect of butanol on the membrane fluidity of intact cells of *Clostridium acetobutylicum*. Appl. Environ. Microbiol. **55:**2729–2731.
5. **Bajad, S. U., et al.** 2006. Separation and quantitation of water soluble cellular metabolites by hydrophilic interaction chromatography-tandem mass spectrometry. J. Chromatogr. A **1125:**76–88.
6. **Bennett, B. D., et al.** 2009. Absolute metabolite concentrations and implied enzyme active site occupancy in *Escherichia coli*. Nat. Chem. Biol. **5:**593–599.
7. **Bennett, B. D., J. Yuan, E. H. Kimball, and J. D. Rabinowitz.** 2008. Absolute quantitation of intracellular metabolite concentrations by an isotope ratio-based approach. Nat. Protoc. **3:**1299–1311.
8. **Boer, V. M., C. A. Crutchfield, P. H. Bradley, D. Botstein, and J. D. Rabinowitz.** Growth-limiting intracellular metabolites in yeast growing under diverse nutrient limitations. Mol. Biol. Cell **21:**198–211.
9. **Boynton, Z. L., G. N. Bennett, and F. B. Rudolph.** 1994. Intracellular concentrations of coenzyme A and its derivatives from *Clostridium acetobutylicum* ATCC 824 and their roles in enzyme regulation. Appl. Environ. Microbiol. **60:**39–44.
10. **Carrieri, D., et al.** 2009. Identification and quantification of water-soluble metabolites by cryoprobe-assisted nuclear magnetic resonance spectroscopy applied to microbial fermentation. Magn. Reson. Chem. **47**(Suppl. 1)**:**S138–S146.
11. **Crown, S. B., et al.** Resolving the TCA cycle and pentose-phosphate pathway of *Clostridium acetobutylicum* ATCC 824: isotopomer analysis, in vitro activities and expression analysis. Biotechnol. J. **6:**300–305.
12. **Dürre, P.** 2005. Handbook on clostridia. Taylor & Francis, Boca Raton, FL.
13. **Durre, P., et al.** 2002. Transcriptional regulation of solventogenesis in *Clostridium acetobutylicum*. J. Mol. Microbiol. Biotechnol. **4:**295–300.
14. **Eisen, M. B., P. T. Spellman, P. O. Brown, and D. Botstein.** 1998. Cluster analysis and display of genome-wide expression patterns. Proc. Natl. Acad. Sci. U. S. A. **95:**14863–14868.
15. **Feng, X. J., et al.** 2004. Optimizing genetic circuits by global sensitivity analysis. Biophys. J. **87:**2195–2202.
16. **Feng, X. J., and H. Rabitz.** 2004. Optimal identification of biochemical reaction networks. Biophys. J. **86:**1270–1281.
17. **Girbal, L., and P. Soucaille.** 1994. Regulation of *Clostridium acetobutylicum* metabolism as revealed by mixed-substrate steady-state continuous cultures: role of NADH/NAD ratio and ATP pool. J. Bacteriol. **176:**6433–6438.
18. **Green, E. M., et al.** 1996. Genetic manipulation of acid formation pathways by gene inactivation in *Clostridium acetobutylicum* ATCC 824. Microbiology **142**(Pt. 8)**:**2079–2086.
19. **Grupe, H., and G. Gottschalk.** 1992. Physiological events in *Clostridium acetobutylicum* during the shift from acidogenesis to solventogenesis in continuous culture and presentation of a model for shift induction. Appl. Environ. Microbiol. **58:**3896–3902.
20. **Harris, L. M., R. P. Desai, N. E. Welker, and E. T. Papoutsakis.** 2000. Characterization of recombinant strains of the *Clostridium acetobutylicum* butyrate kinase inactivation mutant: need for new phenomenological models for solventogenesis and butanol inhibition? Biotechnol. Bioeng. **67:**1–11.
21. **Huang, H., H. Liu, and Y. R. Gan.** Genetic modification of critical enzymes and involved genes in butanol biosynthesis from biomass. Biotechnol. Adv. **28:**651–657.
22. **Hutkins, R. W., and E. R. Kashket.** 1986. Phosphotransferase activity in *Clostridium acetobutylicum* from acidogenic and solventogenic phases of growth. Appl. Environ. Microbiol. **51:**1121–1123.
23. **Hwang, T. L., and A. J. Shaka.** 1995. Water suppression that works: excitation sculpting using arbitrary wave-forms and pulsed-field gradients. J. Magn. Reson. **112:**275–279.
24. **Janssen, H., et al.** A proteomic and transcriptional view of acidogenic and solventogenic steady-state cells of *Clostridium acetobutylicum* in a chemostat culture. Appl. Microbiol. Biotechnol. **87:**2209–2226.
25. **Jiang, Y., et al.** 2009. Disruption of the acetoacetate decarboxylase gene in solvent-producing *Clostridium acetobutylicum* increases the butanol ratio. Metab. Eng. **11:**284–291.
26. **Jones, S. W., et al.** 2008. The transcriptional program underlying the physiology of clostridial sporulation. Genome Biol. **9:**R114.
27. **Kimball, E., and J. D. Rabinowitz.** 2006. Identifying decomposition products in extracts of cellular metabolites. Anal. Biochem. **358:**273–280.
28. **Kraml, C. M., D. Zhou, N. Byrne, and O. McConnell.** 2005. Enhanced chromatographic resolution of amine enantiomers as carbobenzyloxy derivatives in high-performance liquid chromatography and supercritical fluid chromatography. J. Chromatogr. A **1100:**108–115.
29. **LePage, C., M. Fayolle, M. Hermann, and J. P. Vandecasteele.** 1987. Changes in membrane-lipid composition of *Clostridium acetobutylicum* during acetone butanol fermentation: effects of solvents, growth temperature and pH. J. Gen. Microbiol. **133:**103–110.
30. **Lu, W., B. D. Bennett, and J. D. Rabinowitz.** 2008. Analytical strategies for LC-MS-based targeted metabolomics. J. Chromatogr. B Anal. Technol. Biomed. Life Sci. **871:**236–242.
31. **Lu, W., et al.** Metabolomic analysis via reversed-phase ion-pairing liquid chromatography coupled to a stand alone OrbiTrap mass spectrometer. Anal. Chem. **82:**3212–3221.
32. **Mansilla, M. C., L. E. Cybulski, D. Albanesi, and D. de Mendoza.** 2004. Control of membrane lipid fluidity by molecular thermosensors. J. Bacteriol. **186:**6681–6688.

33. **Monot, F., J. Engasser, and H. Petitdemange.** 1984. Influence of pH and undissociated butyric acid on the production of acetone and butanol in batch cultures of *Clostridium acetobutylicum*. Appl. Microbiol. Biotechnol. **19:**422–426.
34. **Monot, F., J. R. Martin, H. Petitdemange, and R. Gay.** 1982. Acetone and butanol production by *Clostridium acetobutylicum* in a synthetic medium. Appl. Environ. Microbiol. **44:**1318–1324.
35. **Munger, J., et al.** 2008. Systems-level metabolic flux profiling identifies fatty acid synthesis as a target for antiviral therapy. Nat. Biotechnol. **26:**1179–1186.
36. **Rabinowitz, J. D., and E. Kimball.** 2007. Acidic acetonitrile for cellular metabolome extraction from *Escherichia coli*. Anal. Chem. **79:**6167–6173.
37. **Rao, G., and R. Mutharasan.** 1989. NADH levels and solventogenesis in *Clostridium acetobutylicum*: new insights through culture fluorescence. Appl. Biochem. Biotechnol. **30:**59–66.
38. **Saldanha, A. J.** 2004. Java Treeview: extensible visualization of microarray data. Bioinformatics **20:**3246–3248.
39. **Schaffer, S., N. Isci, B. Zickner, and P. Durre.** 2002. Changes in protein synthesis and identification of proteins specifically induced during solventogenesis in *Clostridium acetobutylicum*. Electrophoresis **23:**110–121.
40. **Terracciano, J. S., and E. R. Kashket.** 1986. Intracellular conditions required for initiation of solvent production by *Clostridium acetobutylicum*. Appl. Environ. Microbiol. **52:**86–91.
41. **Vollherbst-Schneck, K., J. A. Sands, and B. S. Montenecourt.** 1984. Effect of butanol on lipid composition and fluidity of *Clostridium acetobutylicum* ATCC 824. Appl. Environ. Microbiol. **47:**193–194.
42. **Yuan, J., B. D. Bennett, and J. D. Rabinowitz.** 2008. Kinetic flux profiling for quantitation of cellular metabolic fluxes. Nat. Protoc. **3:**1328–1340.
43. **Yuan, J., et al.** 2009. Metabolomics-driven quantitative analysis of ammonia assimilation in *Escherichia coli*. Mol. Syst. Biol. **5:**302.
44. **Zhao, Y., C. A. Tomas, F. B. Rudolph, E. T. Papoutsakis, and G. N. Bennett.** 2005. Intracellular butyryl phosphate and acetyl phosphate concentrations in *Clostridium acetobutylicum* and their implications for solvent formation. Appl. Environ. Microbiol. **71:**530–537.